

Dense Structural Priors for Sparse Functional Landmark Localization in Surgical Videos

Chenyan Jing¹, Hao Ding¹, Lalithkumar Seenivasan¹, Jacob M. Delgado López¹, and Mathias Unberath^{1*}

Johns Hopkins University, Baltimore, MD, USA
{cjing5, unberath}@jhu.edu

Abstract. Vision foundation models such as SAM 3 can provide transferable object-level structure across diverse surgical video conditions, but segmentation outputs do not explicitly encode the action-conditioned semantics that define functional surgical landmarks. Estimating instrument extent and geometry differs from localizing the tip or anchor relevant to clipping, grasping, or dissecting. We investigate vision foundation model-enabled sparse action-aware landmark localization, using zero-shot, point-prompted structural masks to provide dense instrument-level context without manual pixel-level mask annotations. We propose a lightweight refinement framework that uses SAM 3 as a structural prior. A coarse multi-frame network predicts tip and anchor prompts, generating non-oracle masks that are fused with visual and heatmap features to refine functional landmark predictions. We compare direct mask-augmented supervision, prediction-derived mask-prior refinement, and auxiliary mask supervision to examine how vision foundation model-derived structure should enter a precision-oriented localization system. Experiments on 7,867 clips from 60 surgical videos spanning YouTube, Cholec80, HeiChole, SurgVU, and CRCDC evaluate the approach under heterogeneous conditions. Without manual pixel-level mask annotations for training, the proposed model achieves overall F1 scores of 72.4% for tip and 58.0% for anchor localization. Directly imposing masks on heatmap targets biases learning toward broad tool regions, whereas prediction-derived priors and auxiliary supervision provide effective intermediate structural guidance for action-dependent landmark prediction.

Keywords: Surgical tool landmark localization · Foundation models · Segment Anything Model 3 · Surgical video analysis

1 Introduction

Accurate localization of surgical tool landmarks is important for instrument pose estimation [19], motion analysis and surgical skill assessment [8], and computer-assisted interventions and surgical robotics [10]. We focus on sparse tip and

* Corresponding author

anchor landmarks for clipping, grasping, and dissecting actions, whose locations depend on the active tool and ongoing surgical action. Unlike generic instrument detection, these landmarks encode action-dependent functional locations rather than only instrument presence.

Localization is challenging under occlusion, smoke, specular reflection, motion blur, ambiguous boundaries, and multiple visible instruments [10]. Vision foundation models such as SAM 2 [12], and SAM 3 [3] can provide instrument-level masks from sparse prompts, capturing extent, shape, and coarse spatial continuity. Their medical and surgical adaptations have also shown promise for instrument segmentation [9, 17, 21, 14]. Zero-shot SAM 3 masks are appealing for heterogeneous surgical videos, where pixel-level annotations are costly to obtain.

However, object-level masks do not directly identify the action-relevant tip or anchor. This creates a gap between the broad geometry provided by vision foundation models and the fine-grained functional precision required for landmark localization [5]. Although surgical instrument segmentation has been extensively studied in robotic and laparoscopic videos [6, 1, 2, 22, 13], it remains unclear how foundation-model masks should be incorporated into heatmap-based landmark localization. Direct mask targets may bias predictions toward broad tool regions, whereas landmark prediction requires sharp, spatially specific, and action-relevant responses.

In this work, we formulate sparse functional landmark localization as a vision foundation model-enabled refinement problem. Coarse landmark predictions prompt SAM 3 to obtain non-oracle mask priors, which are fused with visual and heatmap features in a lightweight refinement network. We compare direct mask-augmented supervision, prediction-derived mask-prior refinement, and auxiliary mask supervision. Our results show that dense structural information is most effective as intermediate refinement guidance rather than a direct heatmap target.

2 Method

2.1 Overview

All experiments use a multi-frame heatmap localization backbone adapted from MFCNet [4]. Given a clip centered at frame I_t , $\{I_{t-k}, \dots, I_t, \dots, I_{t+k}\}$, the model predicts action-dependent surgical tool landmark heatmaps on the center frame rather than a future frame. We use the coarse backbone as the common localization model across all compared strategies. The main refinement framework is described in Section 2.2 and 2.3, while direct mask-augmented supervision is introduced separately in Section 2.4.

2.2 Main Framework: Mask-Prior Refinement

Our main framework uses SAM 3 as a zero-shot structural prior rather than as a final landmark predictor. The coarse network predicts center-frame tip and

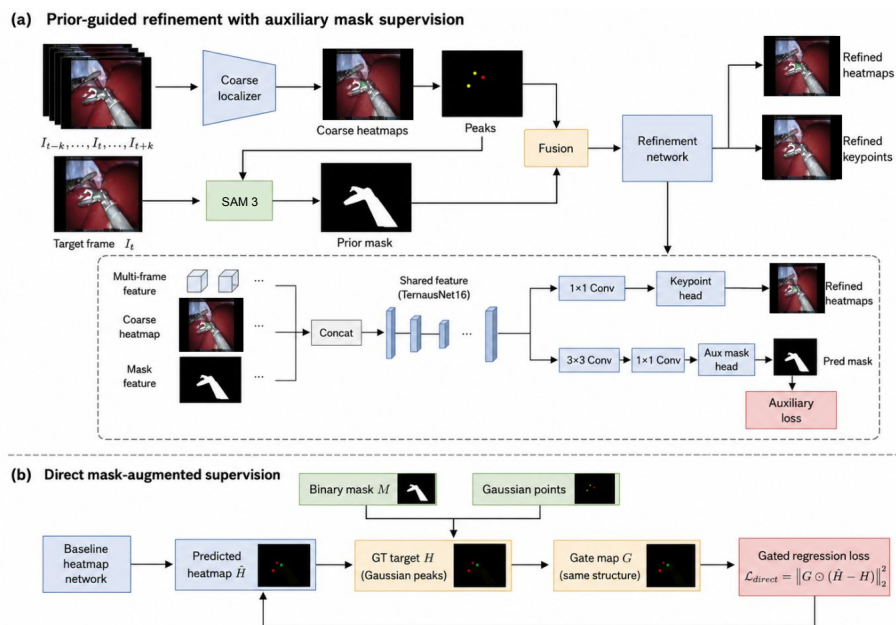


Fig. 1. Overview of the proposed framework and ablation settings. (a) A lightweight task-specific adapter uses coarse landmark predictions to prompt zero-shot SAM 3 and converts the resulting instrument-level structural prior into refined action-dependent landmark heatmaps. (b) Direct mask-augmented supervision uses dense structure as part of the heatmap target, serving as an ablation of target-level structural integration.

anchor heatmaps \hat{H}^c , from which the decoded tip and anchor locations are jointly used as positive prompts for SAM 3. This produces a non-oracle instrument mask M^c , since the prompts come from model predictions rather than ground-truth landmarks.

The refinement network fuses the target-frame visual feature, coarse heatmap feature, and SAM 3-generated mask-prior feature to predict refined heatmaps:

$$\hat{H}^r = F_{\text{refine}}(I_t, \hat{H}^c, M^c).$$

2.3 Auxiliary Supervision and Training Objective

The refinement network can optionally include an auxiliary mask branch during training. As shown in Fig. 1(a), this branch is attached to the shared refinement feature after input fusion, rather than to the final keypoint prediction head. It predicts the SAM 3-generated mask prior M^c , encouraging mask-shape information in the shared feature representation without requiring the final keypoint head to regress the broad mask region. The refinement model is trained using a keypoint heatmap loss, and when the auxiliary branch is included, it also

incorporates an additional mask prediction loss:

$$L = \left\| \hat{H}^r - H^{gt} \right\|_2^2 + \lambda_{\text{aux}} \left\| \hat{M} - M^c \right\|_2^2.$$

Here, H^{gt} denotes the Gaussian ground-truth heatmaps, \hat{M} is the predicted auxiliary mask, and λ_{aux} controls the auxiliary loss weight. For refinement without auxiliary supervision, $\lambda_{\text{aux}} = 0$. The direct mask-augmented ablation is trained separately using L_{direct} .

2.4 Ablation: Direct Mask-Augmented Supervision

As an ablation, we directly inject ground-truth active-instrument mask structure into the heatmap target without using SAM 3 prompting or refinement. The baseline heatmap network is unchanged, but the Gaussian-only target is replaced by a mask-augmented target \tilde{H} , defined as

$$\tilde{H}(x) = \begin{cases} P(x), & x \in \Omega_{\text{kpt}}, \\ \alpha, & M(x) = 1 \text{ and } x \notin \Omega_{\text{kpt}}, \\ 0, & M(x) = 0, \end{cases}$$

where M is the binary tool mask, P denotes the Gaussian keypoint maps, Ω_{kpt} denotes keypoint-centered regions, and $\alpha = 0.1$. This target creates a weak mask plateau with Gaussian keypoint peaks on the tool region and zero background. To prevent the mask plateau from dominating the localization objective, we apply a gated regression loss,

$$L_{\text{direct}} = \left\| G \odot (\hat{H}^d - \tilde{H}) \right\|_2^2,$$

where G uses the same spatial partition as \tilde{H} but assigns separate loss weights to keypoint, mask, and background regions, with the largest weights on keypoint regions.

3 Experimental Setup

3.1 Dataset

We evaluate an internally assembled surgical tool landmark localization dataset of 7,867 clips from 60 videos collected from YouTube, Cholec80 [15], HeiChole [16], SurgVU [23], and CRCO [11]. Each clip represents a surgical action instance and may include multiple visible tools. Annotations specify the active tool, action, tool type, tip, and anchor point. We evaluate clipping with clip applicators, grasping with graspers, and dissecting with hook instruments; cut and scissor sequences are excluded due to limited data. Splits are performed at the surgical-video level to avoid clip-level leakage, with 6,403, 79, and 1,385 clips for training, validation, and testing, respectively. Although the localization model is

Table 1. Dataset distribution by action and source (clip counts). Number of cases per source: YouTube 7, Cholec80 25, HeiChole 7, SurgVU 13, CRCDC 8. The overall train/validation/test split is 6,403/79/1,385.

Action	YouTube	Cholec80	HeiChole	SurgVU	CRCDC	Total
Clip	36	157	57	35	0	285
Dissect	611	3605	939	245	628	6028
Grasp	124	752	220	322	136	1554
Total	771	4514	1216	602	764	7867

trained on video-level splits from multiple sources, SAM 3 mask priors are generated zero-shot and require no source-specific pixel-level mask annotations. This provides transferable structural guidance across heterogeneous surgical videos. Dataset composition is summarized in Table 1.

3.2 Training, Evaluation, and Compared Methods

For external comparisons, we evaluate precision, recall, F1 score, and mean Euclidean localization error under a 15-pixel matching tolerance. We compare our approach with SimpleBaseline [18], YOLOv8-pose [20], and RTMPose [7]. Predictions associated with visually prominent but action-irrelevant instruments are treated as incorrect.

For evaluation, predicted and ground-truth landmarks are matched using a one-to-one matching protocol. A prediction is considered correct when it has the same landmark type and lies within 15 pixels of a ground-truth point. Unmatched predictions are counted as false positives, whereas unmatched ground-truth landmarks are counted as false negatives.

4 Results and Discussion

4.1 Comparison with External Baselines

Table 2 compares our prior-guided refinement model with SimpleBaseline [18], YOLOv8-pose [20], and RTMPose [7].

Our method achieves the highest overall F1 score for both tip and anchor localization. It obtains 72.4% F1 for tips and 58.0% F1 for anchors, indicating improved overall detection performance across the evaluated actions. The method achieves the strongest results for tip localization in the clip and grasp settings, while YOLOv8-pose obtains the highest tip F1 for dissecting sequences.

For anchor localization, our method achieves the best overall F1 despite variation across actions. RTMPose produces slightly lower localization errors in the overall comparison, whereas the proposed method provides higher overall F1 scores for both landmark types.

Table 2. External comparison at a 15-pixel matching tolerance. Precision (P), recall (R), and F1 are reported in percentage; L2 denotes Euclidean localization error in pixels. Higher P/R/F1 and lower L2 are better.

Model	Method	Tip localization				Anchor localization			
		P↑	R↑	F1↑	L2↓	P↑	R↑	F1↑	L2↓
<i>Clip</i>									
SimpleBaseline	Heatmap	93.3	25.5	40.1	8.88	70.1	17.8	28.8	11.61
YOLOv8-pose	Top-down	47.1	26.2	33.6	8.02	65.6	51.2	51.2	6.54
RTMPose	Top-down	50.2	50.2	50.2	12.73	49.3	49.4	49.4	9.07
Ours	Prior + aux refinement	77.9	48.4	59.7	9.05	61.5	51.1	55.8	10.19
<i>Grasp</i>									
SimpleBaseline	Heatmap	88.4	39.1	54.2	8.96	63.2	25.9	45.8	12.31
YOLOv8-pose	Top-down	52.5	31.5	39.4	10.52	60.4	43.4	50.5	11.50
RTMPose	Top-down	58.7	58.7	58.7	7.29	35.8	35.8	35.8	7.39
Ours	Prior + aux refinement	80.9	49.7	61.6	7.23	56.2	41.6	47.8	10.36
<i>Dissect</i>									
SimpleBaseline	Heatmap	46.4	26.4	33.6	14.97	78.2	39.9	52.8	10.49
YOLOv8-pose	Top-down	84.7	72.2	78.0	10.04	52.6	45.2	48.6	12.02
RTMPose	Top-down	69.3	68.8	69.1	8.90	59.1	59.4	59.2	8.28
Ours	Prior + aux refinement	81.1	72.6	76.6	10.47	67.6	52.2	58.9	8.49
<i>Overall</i>									
SimpleBaseline	Heatmap	53.1	28.5	37.1	13.38	77.3	39.4	52.2	10.58
YOLOv8-pose	Top-down	77.4	60.1	67.7	10.05	53.3	45.0	48.8	11.89
RTMPose	Top-down	65.5	65.2	65.4	8.70	57.0	57.2	57.1	8.25
Ours	Prior + aux refinement	81.0	65.5	72.4	9.80	66.6	51.3	58.0	8.64

4.2 Bridging Structural Generalization and Functional Precision

Table 3 examines how SAM 3-derived structural information should be incorporated into sparse, action-aware landmark localization. We compare direct mask-augmented targets with refinement-based use of prediction-derived mask priors and auxiliary mask supervision.

For tip localization, coarse-to-refine prediction improves overall F1 from 52.9% to 68.5%. Adding the SAM 3 mask prior further increases F1 to 71.6%, and the full model with auxiliary supervision achieves the best result of 72.4%. Direct mask-augmented supervision also improves tip localization to 68.7%, indicating that structural cues are useful, but it remains below the prior-guided refinement variants.

For anchor localization, refinement improves F1 from 51.5% to 56.4%, while the mask prior further improves it to 57.9%. The full model reaches the best anchor F1 of 58.0% and reduces L2 error from 8.85 to 8.64 pixels compared with refinement plus prior alone. In contrast, direct mask-augmented supervision

Table 3. Internal ablation of mask-guided refinement strategies. Detection precision, recall, and F1 are evaluated at a 15-pixel matching threshold. L2 denotes the average localization error in pixels.

Method	LM	Clip		Grasp		Dissect		Overall			
		F1↑	L2↓	F1↑	L2↓	F1↑	L2↓	P↑	R↑	F1↑	L2↓
Coarse	Tip	53.4	9.02	60.5	7.40	51.7	10.44	61.1	46.7	52.9	9.92
	Anchor	45.9	9.30	46.5	10.49	51.8	8.26	67.3	41.7	51.5	8.36
Refine w/o prior	Tip	57.9	8.59	61.6	7.23	71.4	10.76	76.0	62.4	68.5	9.96
	Anchor	54.0	11.17	47.9	10.39	57.2	8.29	63.1	50.9	56.4	8.49
Direct mask-aug.	Tip	57.4	9.16	64.1	7.32	74.7	10.12	72.9	65.0	68.7	8.95
	Anchor	43.4	12.82	44.9	9.88	59.6	8.45	58.4	54.6	56.4	8.78
Refine + prior	Tip	58.5	7.98	61.6	7.21	75.7	10.65	80.3	64.7	71.6	9.87
	Anchor	63.8	10.69	47.5	10.16	58.7	8.71	66.3	51.4	57.9	8.85
Refine + prior + aux	Tip	59.7	9.05	61.6	7.23	76.6	10.47	81.0	65.5	72.4	9.80
	Anchor	55.8	10.20	47.8	10.36	58.9	8.49	66.6	51.3	58.0	8.64

reaches 56.4% F1 despite higher recall, suggesting that dense mask targets can bias predictions toward broad tool regions.

Overall, the results suggest that broad structural coverage and precise functional localization are better handled separately. Prediction-derived mask priors provide useful instrument-level context during refinement, while preserving sparse, action-dependent heatmap targets for final landmark prediction.

4.3 Action- and Landmark-Dependent Analysis

The effect of mask guidance varies across actions and landmark types. For clipping, refinement-level mask guidance is especially beneficial for anchor localization: the mask-prior refinement model reaches 63.8% anchor F1, compared with 45.9% for the coarse baseline and 43.4% for direct mask-augmented supervision. For dissecting, the full model yields the strongest and most consistent performance, with 76.6% tip F1 and 58.9% anchor F1. In contrast, grasping shows weaker gains from mask guidance. This may be because grasping scenes often contain multiple visible instruments, while annotations are defined only for the active tool. This result highlights the distinction between object-level structural quality and action-dependent functional relevance. Even a plausible mask prior may be insufficient when it is not semantically aligned with the active instrument and surgical action, motivating the need for a task-specific adapter rather than direct reliance on segmentation output.

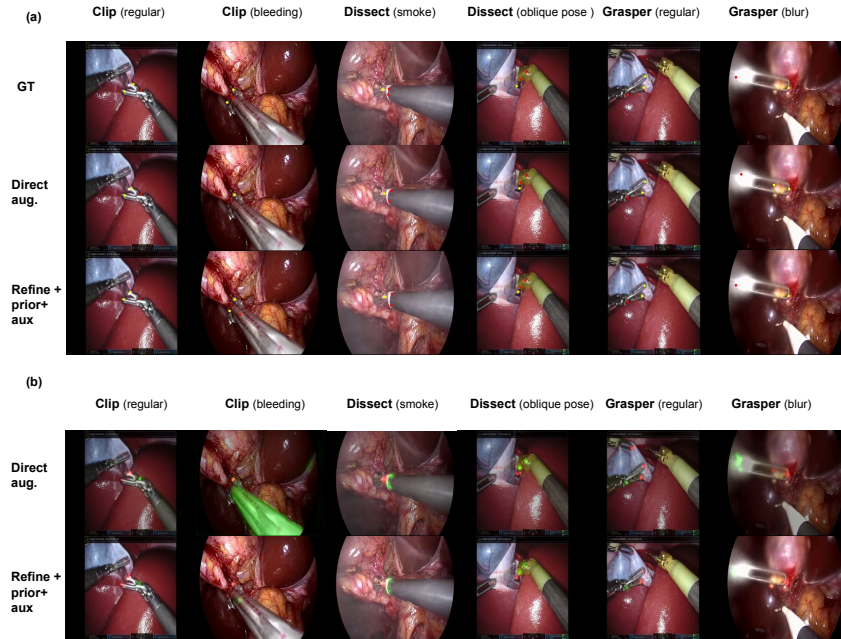


Fig. 2. Qualitative comparison illustrating the tension between broad structural coverage and sharp functional localization. Direct mask-augmented supervision produces broader tool-region activations, whereas the proposed prior-guided adapter preserves localized responses around action-relevant landmarks while leveraging SAM 3-derived structural context.

4.4 Qualitative Results

Figure 2 compares keypoint predictions and heatmap responses under representative surgical conditions, including bleeding, smoke, oblique tool pose, and motion blur. The examples highlight the gap between broad instrument-level coverage and precise action-dependent landmark localization. Direct mask-augmented supervision captures the visible instrument region but often produces broader activations because dense mask structure is imposed on the target representation. In contrast, prior-guided refinement retains sharper responses around action-relevant landmarks while leveraging mask-derived context. These examples support the use of dense structure as refinement guidance rather than a replacement for sparse keypoint heatmaps.

5 Conclusion

This work studies how dense mask-derived structural priors can be incorporated into sparse functional landmark localization for surgical tools. Our results show

that mask information is useful, but its benefit depends on how it is introduced. Directly inserting masks into the heatmap target improves over the coarse baseline, yet the resulting broad mask plateau can bias learning toward tool regions rather than precise keypoint peaks. Rather than treating SAM 3 masks as direct landmark targets, our results show that zero-shot foundation-model geometry is most effective when adapted as intermediate context by a lightweight task-specific refinement network. This enables transferable instrument-level structure to support precise, action-dependent surgical landmark localization without requiring manual pixel-level mask annotations.

References

1. Allan, M., Shvets, A., Kurmann, T., Zhang, Z., Duggal, R., Su, Y.H., Rieke, N., Laina, I., Kalavakonda, N., Bodenstedt, S., et al.: 2017 robotic instrument segmentation challenge. arXiv preprint arXiv:1902.06426 (2019). <https://doi.org/10.48550/arXiv.1902.06426>
2. Allan, M., et al.: 2018 robotic scene segmentation challenge. arXiv preprint arXiv:2001.11190 (2020). <https://doi.org/10.48550/arXiv.2001.11190>
3. Carion, N., Gustafson, L., Hu, Y.T., Debnath, S., Hu, R., Suris, D., Ryali, C., Alwala, K.V., Khedr, H., Huang, A., Lei, J., Ma, T., Guo, B., Kalla, A., Marks, M., Greer, J., Wang, M., Sun, P., Rädle, R., Afouras, T., Mavrouti, E., Xu, K., Wu, T.H., Zhou, Y., Momeni, L., Hazra, R., Ding, S., Vaze, S., Porcher, F., Li, F., Li, S., Kamath, A., Cheng, H.K., Dollár, P., Ravi, N., Saenko, K., Zhang, P., Feichtenhofer, C.: SAM 3: Segment Anything with Concepts. arXiv preprint arXiv:2511.16719 (2025). <https://doi.org/10.48550/arXiv.2511.16719>
4. Ghanekar, B., Johnson, L.R., Laughlin, J.L., O'Malley, M.K., Veeraraghavan, A.: Video-based surgical tool-tip and keypoint tracking using multi-frame context-driven deep learning models. In: Proceedings of the IEEE International Symposium on Biomedical Imaging (ISBI) (2025)
5. Hariharan, B., Arbeláez, P., Girshick, R., Malik, J.: Hypercolumns for object segmentation and fine-grained localization. In: Proceedings of the IEEE Conference on Computer Vision and Pattern Recognition. pp. 447–456 (2015)
6. Hong, W.Y., Kao, C.L., Kuo, Y.H., Wang, J.R., Chang, W.L., Shih, C.Y.: CholecSeg8k: A semantic segmentation dataset for laparoscopic cholecystectomy based on Cholec80. arXiv preprint arXiv:2012.12453 (2020). <https://doi.org/10.48550/arXiv.2012.12453>
7. Jiang, T., Lu, P., Zhang, L., Ma, N., Han, R., Lyu, C., Li, Y., Chen, K.: RTM-Pose: Real-time multi-person pose estimation based on MMPose. arXiv preprint arXiv:2303.07399 (2023). <https://doi.org/10.48550/arXiv.2303.07399>
8. Law, H., Ghani, K., Deng, J.: Surgeon technical skill assessment using computer vision based analysis. In: Proceedings of the 2nd Machine Learning for Healthcare Conference. Proceedings of Machine Learning Research, vol. 68, pp. 88–99. PMLR (2017)
9. Ma, J., He, Y., Li, F., Han, L., You, C., Wang, B.: Segment anything in medical images. *Nature Communications* **15**, 654 (2024). <https://doi.org/10.1038/s41467-024-44824-z>
10. Nema, S., Vachhani, L.: Surgical instrument detection and tracking technologies: Automating dataset labeling for surgical skill assessment. *Frontiers in Robotics and AI* **9**, 1030846 (2022). <https://doi.org/10.3389/frobt.2022.1030846>

11. Oh, K.H., Borgioli, L., Mangano, A., Valle, V., Pangrazio, M.D., Toti, F., Pozza, G., Ambrosini, L., Ducas, A., Žefran, M., et al.: Expanded comprehensive robotic cholecystectomy dataset (CRCDD). arXiv preprint arXiv:2412.12238 (2024)
12. Ravi, N., Gabeur, V., Hu, Y.T., Hu, R., Ryali, C., Ma, T., Khedr, H., Rädle, R., Rolland, C., Gustafson, L., Mintun, E., Pan, J., Alwala, K.V., Carion, N., Wu, C.Y., Girshick, R., Dollár, P., Feichtenhofer, C.: SAM 2: Segment anything in images and videos. arXiv preprint arXiv:2408.00714 (2024)
13. Rueckert, T., Rueckert, D., Palm, C.: Methods and datasets for segmentation of minimally invasive surgical instruments in endoscopic images and videos: A review of the state of the art. arXiv preprint arXiv:2304.13014 (2023). <https://doi.org/10.48550/arXiv.2304.13014>
14. Sheng, Y., Bano, S., Clarkson, M.J., Islam, M.: Surgical-DeSAM: Decoupling SAM for instrument segmentation in robotic surgery. *International Journal of Computer Assisted Radiology and Surgery* (2024). <https://doi.org/10.1007/s11548-024-03163-6>
15. Twinanda, A.P., Shehata, S., Mutter, D., Marescaux, J., de Mathelin, M., Padoy, N.: EndoNet: A deep architecture for recognition tasks on laparoscopic videos. *IEEE Transactions on Medical Imaging* **36**(1), 86–97 (2017). <https://doi.org/10.1109/TMI.2016.2593957>
16. Wagner, M., Müller-Stich, B.P., Kisilenko, A., Tran, D., Heger, P., Mündermann, L., Lubotsky, D., Müller, B., Davitashvili, T., Capek, M., et al.: Comparative validation of machine learning algorithms for surgical workflow and skill analysis with the HeiChole benchmark. *Medical Image Analysis* **86**, 102770 (2023). <https://doi.org/10.1016/j.media.2023.102770>
17. Wang, A., Islam, M., Xu, M., Zhang, Y., Ren, H.: SAM meets robotic surgery: An empirical study on generalization, robustness and adaptation. arXiv preprint arXiv:2308.07156 (2023). <https://doi.org/10.48550/arXiv.2308.07156>
18. Xiao, B., Wu, H., Wei, Y.: Simple baselines for human pose estimation and tracking. In: *Proceedings of the European Conference on Computer Vision*. pp. 466–481 (2018)
19. Xu, H., Weld, A., Xu, C., Roddan, A., Cartucho, J., Karaoglu, M.A., Ladikos, A., Li, Y., Li, Y., Shen, D., Yang, S., Lee, G., Park, S., Shin, J., Kim, Y.G., Fothergill, L., Jones, D., Valdastrì, P., Sarikaya, D., Giannarou, S.: SurgRIPE challenge: Benchmark of surgical robot instrument pose estimation. *Medical Image Analysis* **105**, 103674 (2025). <https://doi.org/10.1016/j.media.2025.103674>
20. Yaseen, M.: What is YOLOv8: An in-depth exploration of the internal features of the next-generation object detector. arXiv preprint arXiv:2408.15857 (2024)
21. Yue, W., Zhang, J., Hu, K., Xia, Y., Luo, J., Wang, Z.: SurgicalSAM: Efficient class promptable surgical instrument segmentation. In: *Proceedings of the AAAI Conference on Artificial Intelligence*. vol. 38, pp. 7300–7308 (2024). <https://doi.org/10.1609/aaai.v38i7.28514>
22. Zhao, Z., Voros, S., Weng, Y., Chang, F., Li, R.: Tracking-by-detection of surgical instruments in minimally invasive surgery via the convolutional neural network deep learning-based method. *Computer Assisted Surgery* **22**(sup1), 26–35 (2017). <https://doi.org/10.1080/24699322.2017.1378777>
23. Zia, A., Berniker, M., Nespolo, R., Perreault, C., Wang, Z., Mueller, B., Schmidt, R., Bhattacharyya, K., Liu, X., Jarc, A.: Surgical visual understanding (SurgVU) dataset. arXiv preprint arXiv:2501.09209 (2025)